Journal of Nuclear Materials 401 (2010) 17–24

Contents lists available at ScienceDirect

Journal of Nuclear Materials

journal homepage: www.elsevier.com/locate/jnucmat

Ratcheting and low cycle fatigue behavior of SA333 steel and their life prediction

Surajit Kumar Paul [a,*], S. Sivaprasad [a], S. Dhar [b], S. Tarafder [a]

[a] Materials Science & Technology Division, National Metallurgical Laboratory (Council of Scientific & Industrial Research), Jamshedpur 831 007, India
[b] Department of Mechanical Engineering, Jadavpur University, Kolkata 700 032, India

ARTICLE INFO

Article history:
Received 8 December 2009
Accepted 18 March 2010

ABSTRACT

Ratcheting and low cycle fatigue (LCF) experiments have been conducted at 25 °C temperature in laboratory environment under different loading conditions. SA333 steel exhibits cyclic hardening throughout its life during LCF. It is found that ratcheting strain increases with both increasing mean stress and stress amplitude. It has also been noticed that plastic strain amplitude and plastic strain energy decrease with increase in mean stress at constant stress amplitude. Ratcheting and LCF life in the range of 10^2–10^5 cycles have been predicted with the help of a mean stress-based fatigue lifing equation.

1. Introduction

SA333 steel is used as a piping material for pressurized heavy water reactors of nuclear power plants. Typically, piping systems comprise straight pipes, T-joints and elbows that must be designed against failure under operative and accidental conditions. One of the mechanisms through which damage may be incorporated in such piping system is by fatigue. Fatigue damage may be manifested through nominally elastic high cycle fatigue loading accompanying vibrations and by cyclic plastic loading, viz. low cycle fatigue and ratcheting fatigue, due to start-up and shut-down, variation in operating conditions or seismic events. While strain-controlled cyclic plastic excursion is generally termed as low cycle fatigue (LCF), ratcheting is the consequence of asymmetric cyclic plastic loading, usually under stress control. Knowledge of the resistance of materials to damage accumulation and failure under various types of fatigue loading is necessary for efficient design of piping systems. This paper examines low cycle fatigue and ratcheting fatigue behavior of SA333 steel at 25 °C temperature and explores universal representation of its fatigue life under such loading conditions.

With respect to LCF of engineering materials, there is a good appreciation of the underlying lowest-level mechanisms [1–3], leading to development of physics based models [4,5], and availability of knowledge-base for engineering applications [6–12]. Ratcheting fatigue on the other hand is perhaps not as well researched a subject. There is however an increasing recognition of the importance of ratcheting, particularly with respect to damage in pressurized components [13–15], like piping.

Ratcheting can be defined as progressive and directional accumulation of plastic strain due to asymmetrical stress cycling [6,11,16]. In piping systems, it leads to ovalization at elbows and appreciable thinning of pipe-walls [17,18]. Investigations have been carried out to study ratcheting fatigue in specific engineering materials: 1026 carbon steel [16], Elbrodur-NIB copper alloy [11] and 1070 carbon steel [19] for example.

An important issue with respect to LCF and ratcheting is engineering descriptions of fatigue lives. In general, fatigue life relations may be based on stress, strain or energy parameters. Relations based on energy have a potential advantage in that both stress and strain parameters are included in there formulations. However, the use of plastic strain energy as the primary input for life calculation limits the applicability of fatigue life relations as this renders them insensitive to the effect of mean stress [12]. When thermal effects are the primary cause for fatigue, cyclic plasticity can be defined easily in terms of strains, and strain-based approaches to fatigue lifing are found to be adequate. For the greater majority of fatigue situations, cyclic loading in stress controlled, and stress-based fatigue life models are most relevant for engineering applications. Mean stress effects can easily be incorporated into stress-based fatigue lifing models, and they can represent ratcheting fatigue more explicitly.

In this work, stress-based engineering approach to predicting fatigue lives under both LCF and ratcheting fatigue has been employed to demonstrate their effectiveness.

2. Experimental

The SA333 Grade 6 carbon manganese steel used in this study was sourced from piping components (outer diameter 508 mm and wall thickness 50.8 mm) used for primary heat transport in nuclear power plants. The nominal composition of the steel in weight% was: C 0.18%, Mn 0.9%, Si 0.02% and P 0.02%. The microstructure of the material consisted of ferrite–pearlite bands, as shown typically in Fig. 1. The banding was oriented in the direction

* Corresponding author. Tel.: +91 9939632284; fax: +91 6572345213.
E-mail address: paulsurajit@yahoo.co.in (S.K. Paul).

0022-3115/$ - see front matter © 2010 Elsevier B.V. All rights reserved.
doi:10.1016/j.jnucmat.2010.03.014

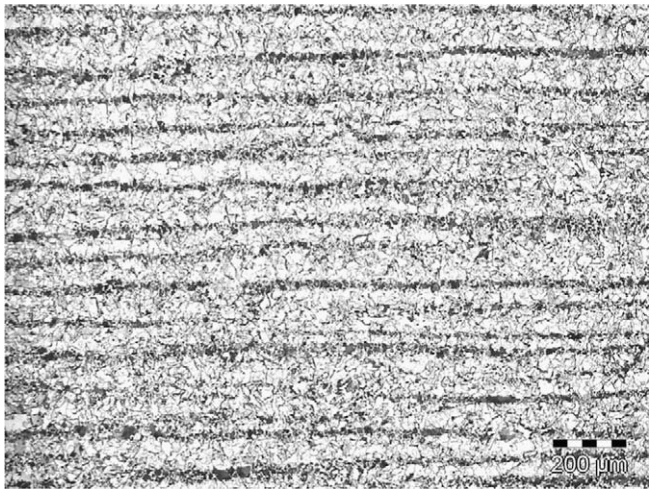

Fig. 1. Ferrite–pearlite banded structure of SA333 steel in optical microscope.

of the pipe axis. Cylindrical specimens of 7 mm gauge diameter and 13 mm parallel length were fabricated from the pipe, with their loading axes parallel to the pipe axis. Tensile, LCF and ratcheting tests were conducted using the specimens, employing a 100 KN closed-loop servo-electric test system. All tests were carried out in ambient laboratory air at room temperature (25 °C). A 12.5 mm gauge length extensometer was used for measuring and controlling strains, as necessary. Test control and test data acquisition was implemented through computers interfaced to test machine controllers. Tensile tests were carried out at a strain rate of $1 \times 10^{-3}\ s^{-1}$ to obtain mechanical properties of material. The tensile properties of the SA333 steel are given in Table 1.

All LCF tests were performed using triangular waveform, under strain control at a constant strain rate of $1 \times 10^{-3}\ s^{-1}$. LCF test details are tabulated in Table 2. Fully reversed strain cycling (strain ratio = −1) was applied for all LCF experiments. Ratcheting tests were conducted under engineering stress control with various combinations of mean stress and stress amplitude, at a constant stress rate of 50 MPa s^{-1}. The stress amplitude and mean stress used in ratcheting test are given in Table 3. For all LCF and ratcheting tests, it was ensured that at least 200 data points were collected in every cycle. All tests were continued till failure. The failure criteria decided for both LCF and ratcheting tests were 50% reduction of maximum load bearing capacity of the specimen.

Table 1
Tensile properties of SA333 steel.

Yield stress (MPa)	Ultimate tensile stress (MPa)	Uniform elongation (%)	Total elongation (%)
304	494	17.18	24.53

Table 2
LCF test conditions and cycles to failure.

S. No.	Strain amplitude (%)	Number of cycles to failure	Saturated stress amplitude (MPa)
1	0.5	2107	349.64
2	0.7	1487	391
3	0.85	769	394.2
4	1.0	801	424
5	1.2	559	428.89
6	1.4	397	455
7	1.6	303	459.5

Table 3
Ratcheting test conditions, cycles to failure, and failure ratcheting strain.

S. No.	Stress amplitude (MPa)	Mean stress (MPa)	Number of cycles to failure	Final ratcheting strain (%)
1	310	40	3199	29.5
2	310	60	2061	56.4
3	310	80	1184	53.2
4	310	120	570	57.2
5	270	80	13,392	31.1
6	350	80	475	44.2

3. Results and discussion

LCF experiments are in order to understand the material responses under strain variation ($\alpha\Delta T$; α is the coefficient of thermal expansion and ΔT is temperature fluctuation) which arises due to temperature alteration. Study of ratcheting is needed where repeated cycles of load excursion is applied with the load cycles not necessarily being symmetric in nature. Ratcheting can deteriorate the performances of a component by the cumulative effects of fatigue damage, which arises from alternating stress, and damage by permanent strain (ratcheting strain) accumulation in a particular direction. The latter leads to further enhancement of fatigue damage by continuous thinning of the component cross-section. Ratcheting strain can be defined as the position of the center of the hysteresis loop on the strain axis. The axial ratcheting strain ε_r can be mathematically expressed as:

$$\varepsilon_r = \frac{1}{2}(\varepsilon_{min} + \varepsilon_{max}) \quad (1)$$

where ε_{max} is the maximum of axial strain and ε_{min} is the minimum axial strain for a particular cycle.

3.1. LCF behavior

Fig. 2 shows the cyclic stress response of SA333 steel observed from LCF tests at various total strain amplitude. SA333 steel, being a ferritic steel, shows continuous hardening throughout its LCF life. At total strain amplitude of ±0.5%, the hardening is barely perceptible. At higher levels of cyclic straining, hardening is rapid in the first few cycles, followed by an almost steady but low rate of hardening until failure is imminent. It may be noted that a saturated state of hardening is not exhibited, except at the lower end of the range of strain amplitudes investigated. This behavior is typical of bcc materials in which the paucity of mobile dislocations preclude complex interactions that lead to extensive hardening.

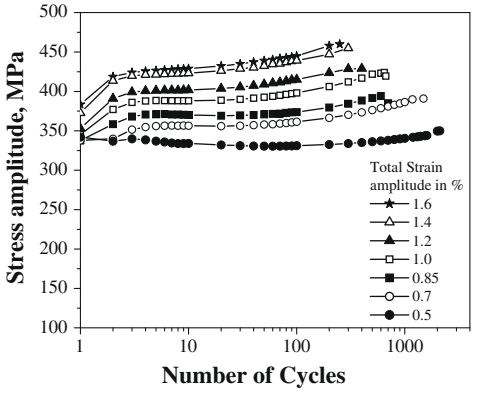

Fig. 2. Stress amplitude verses number of cycles in LCF: at the strain amplitude of ±0.5%, ±0.7%, ±0.85%, ±1.0%, ±1.2%, ±1.4%, and ±1.6%.

Similar observations have been reported for other bcc materials, like [20,21], and also sometimes for fcc materials [1,22]. The almost pure plastic behavior exhibited by SA333 steel at small plastic strains during monotonic deformation (as also during the first quarter cycle of cyclic loading) is a manifestation of this unavailability of mobile dislocations.

Although cyclically stable stress–strain hysteresis loops were not exhibited during LCF of SA333 steel, loops obtained, just prior to initiation of micro-crack (and consequent distortion of the hysteresis loops) can be assumed to represent the ultimate hardened state of the substructure. A set of such stable loops can be used to define the cyclic stress–strain curve, represented by:

$$\varepsilon_a = \frac{\sigma_a^{sat}}{E} + \left(\frac{\sigma_a^{sat}}{K}\right)^{1/n'} \quad (2)$$

where σ_a^{sat} is the stress amplitude of saturated cycle, ε_a is the total strain amplitude, E is the modulus of elasticity, K is the cyclic strain hardening coefficient and n' is the cyclic strain hardening exponent. The value of K and n' are calculated to be 830 MPa and 0.14214 respectively for SA333 steel. The cyclic stress–strain curve is shown in Fig. 3. From the figure, it can be seen that the monotonic stress–strain curve lies below the cyclic stress–strain curve, which indicates that the material undergoes substantial hardening during strain-controlled cycling. In order to quantify the degree of cyclic hardening with respect to the monotonic stress–strain curve, a simple expression of degree of cyclic hardening (H) [10] can be given by:

$$H = \frac{\sigma_a^{sat} - \sigma_a^1}{\sigma_a^1} \quad (3)$$

where σ_a^1 is the stress amplitude in the first cycle. Degree of cyclic hardening (H) is plotted as a function of applied strain amplitudes (ε_a) in Fig. 4. The figure indicates that with increasing applied strain amplitude, the degree of cyclic hardening initially increases and saturates at higher strain amplitude. Similar dependency of cyclic hardening on imposed strain amplitude was also reported for austenitic stainless steels, such as AISI 304L and AISI 316 [23–26].

3.2. Ratcheting behavior

The accumulation of ratcheting strain with number of cycles has been depicted in Fig. 5. This curve is similar to a conventional creep curve, and can be divided into the primary, secondary and tertiary regions. Fundamentally, the deformation mechanisms are vastly different. Ratcheting is associated with dislocation movement, their interactions and cell formations [1], while creep is related to diffusion controlled glide and climb of dislocations, grain boundary sliding and void formation [27]. In engineering stress

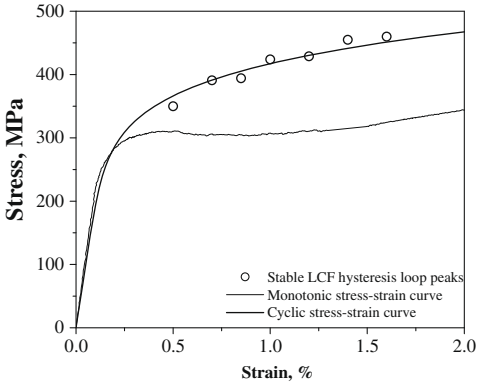

Fig. 3. Cyclic stress–strain curve.

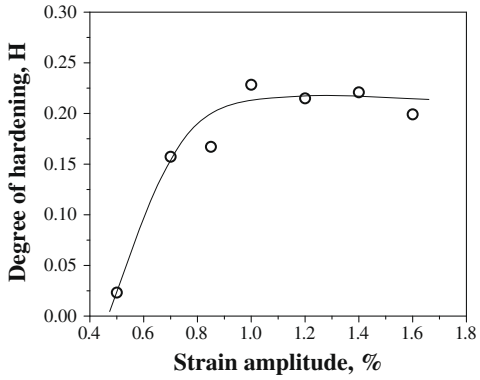

Fig. 4. Degree of hardening (H) vs. strain amplitude.

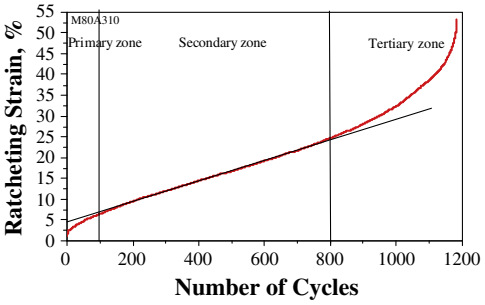

Fig. 5. Ratcheting curve with three distinct zones: at stress amplitude of 310 MPa and mean stress of 80 MPa.

controlled ratcheting, two competitive mechanisms are operative: cyclic hardening [28] and geometrical softening which arises from cross sectional area reduction due to accumulation of permanent strain. As ratcheting strain is small in the primary region, the cross sectional area reduction is also small and as a consequence cyclic hardening dominates. Cyclic hardening plays a key role in ratcheting rate decay in the primary region [29]. In the secondary region there is a balance between cyclic hardening and softening and as a result a steady state ratcheting rate is maintained. Softening dominates in the tertiary region, the ratcheting strain reaching a sufficiently high value to result in substantial cross sectional area reduction. This dimensional alteration of the specimen helps to increase the maximum true stress to such a high value that instability and necking is often observed. Similar trends of ratcheting strain accumulation have been reported for many materials; for example Inconel 718 at 649 °C [30].

Fig. 6a and b shows the accumulation of ratcheting strain with number of cycles for constant stress amplitude and constant mean stress respectively. From these figures it can be seen that ratcheting life decreases and ratcheting strain increases with increase in mean stress or stress amplitude. It was also noted that most of the specimens failed by necking rather than by fatigue crack propagation, which is not a common observation during LCF testing. This type of failure behavior is due to uncontained increase in true stress, given by $\sigma_T = \sigma(1 + \varepsilon_r)$, accompanying accumulation of ratcheting strain ε_r, leading to localization of deformation and necking.

Ratcheting test at a mean stress of 80 MPa and stress amplitude of 310 MPa exhibited 53.18% strain accumulation before failure, as shown in Fig. 5. Ratcheting strain accumulation of 53.18% results in 34.72% area reduction and 1.53 times rise in true stress. The true stress amplitude thus increases uncontrollably while the engineering stress amplitude is maintained at constant value as shown in Fig. 7. True stress and strain are representative of the actual

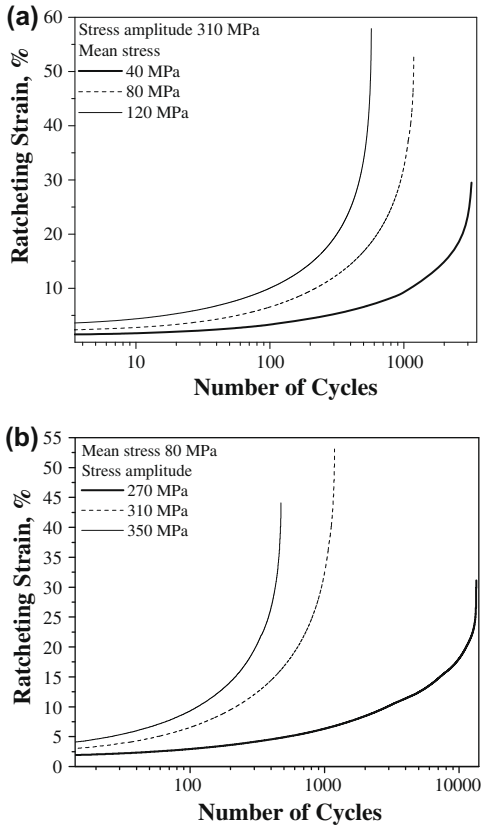

Fig. 6. Ratcheting strain vs. number of cycles: (a) at constant stress amplitude of 310 MPa and mean stress of 40, 80, and 120 MPa (b) at constant mean stress of 80 MPa and stress amplitude of 270, 310, and 350 MPa.

responses of materials. In engineering stress controlled ratcheting tests, the maximum true stress reaches a sufficiently high value that is comparable to the true ultimate tensile stress during a tensile test, and as a result necking becomes inevitable. It is seen from engineering stress controlled ratcheting experiments that the ratcheting strain accumulated and the elongation prior to localization is higher than the uniform elongation during tensile test, which for SA333 steel is 17.18%. The material can thus accommodate much higher strains during ratcheting without necking. Initiation of micro-voids is the probable cause of necking, and their coalescence leads to failure [31,32]. So it may be said that initiation of micro-voids is delayed in case of ratcheting and this leads to high ratcheting strain in engineering stress controlled ratcheting experiments.

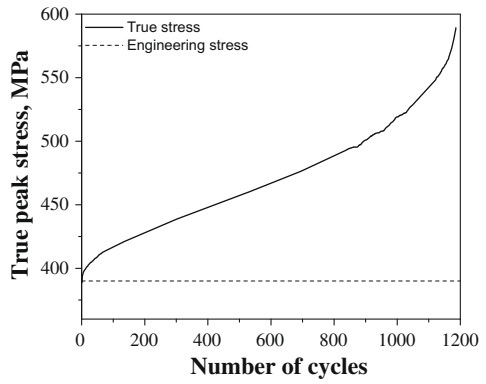

Fig. 7. Variation of maximum true stress with number of cycles in engineering stress controlled ratcheting test at a mean stress of 80 MPa and stress amplitude of 310 MPa.

Ratcheting strain rate for a particular cycle is the amount of non-closure in the hysteresis loop of that cycle. The variation of ratcheting strain rate with life fraction (ratio of number of cycles to the number of cycles to failure) is plotted in Fig. 8a and b. From the figures, it can be seen that the trends of the plots are quite similar: initially in the primary region ratcheting rate decreases; after that in the secondary region ratcheting rate maintains a steady state; and finally ratcheting rate increases uncontrollable, indicating the tertiary region of the ratcheting curve.

Width of the hysteresis loop is generally taken as double of plastic strain amplitude for fully reversed strain cycling. Similarly width of the hysteresis loop measured at mean stress value is considered as double of plastic strain amplitude for ratcheting, shown in Fig. 9a. Fig. 9b and c demonstrates the change of plastic strain amplitude with life fraction at constant stress amplitude and constant mean stress respectively. Change of plastic strain amplitude describes the cyclic hardening/softening of the material under stress controlled cycling. In both the figures it can be seen that plastic strain amplitude decreases in the initial few cycles, followed by a region of steady value and finally raises at very rapidly to give failure. With cyclic hardening, geometric softening due to reduction of cross section area occurs simultaneously, and their combined effects are reflected in plastic strain amplitude variations. It may be noted that lower plastic strain amplitudes are exhibited at higher mean stress in comparison to lower mean stress, as evident from Fig. 9b. Various researchers have showed similar results for different materials, like carbon steel [33,34], 304 stainless steel [35,36], polycrystalline copper [37,38] and polycrystalline nickel [39].

The hysteresis loop area represents the energy that has been put into the material system in any given cycle to contribute the

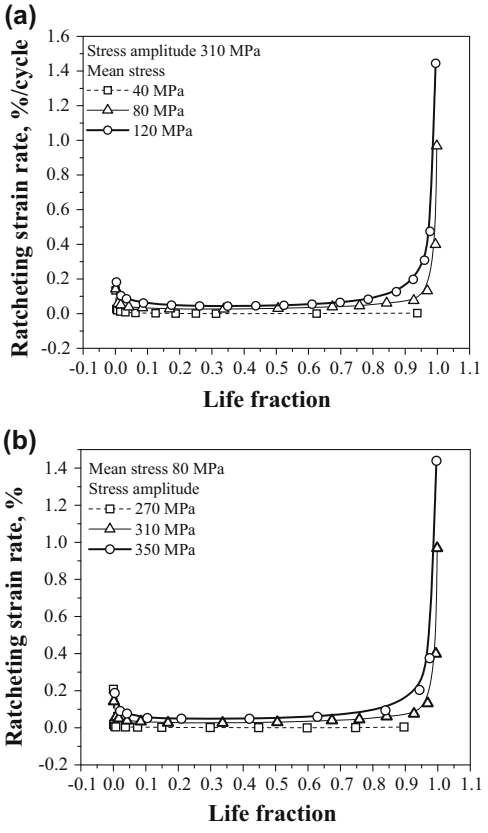

Fig. 8. Ratcheting strain rate vs. life fraction: (a) at constant stress amplitude of 310 MPa and mean stress of 40, 80, and 120 MPa (b) at constant mean stress of 80 MPa and stress amplitude of 270, 310, and 350 MPa.

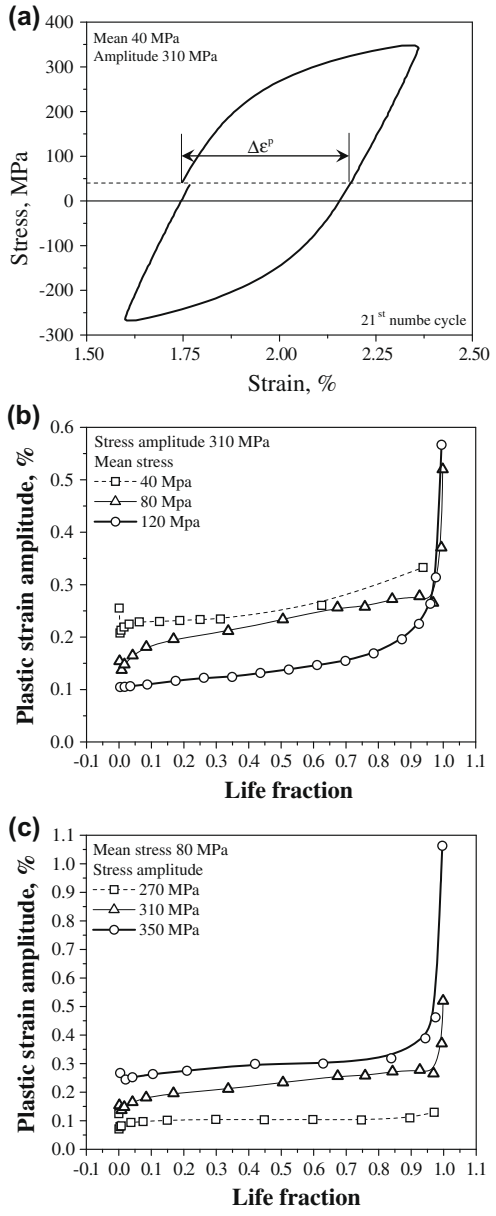

Fig. 9. (a) Plastic strain amplitude in 21st cycle for 40 MPa mean stress and 310 MPa stress amplitude controlled cycling ($\Delta\varepsilon^p$ = double of plastic strain amplitude); plastic strain amplitude vs. life fraction: (b) at constant stress amplitude of 310 MPa and mean stress of 40, 80, and 120 MPa (c) at constant mean stress of 80 MPa and stress amplitude of 270, 310, and 350 MPa.

damage that has accumulated. It is instinctive to study how this area is altered during ratcheting tests. Hysteresis loop area, as a function of life fraction has been plotted in Fig. 10a and b for constant stress amplitude and mean stress respectively. The nature of the curves is similar to that of Fig. 9a and b, i.e. plastic strain amplitude variation with life fraction. Like plastic strain amplitude, hysteresis loop area is also very much sensitive to mean stress. Fig. 10a depicts that hysteresis loop area decreases with increasing mean stress for constant stress amplitude.

3.3. Ratcheting and LCF life prediction by a stress-based fatigue lifing equation

Engineering structures and components are often subjected to cyclic loads superimposed with tensile mean stress during service.

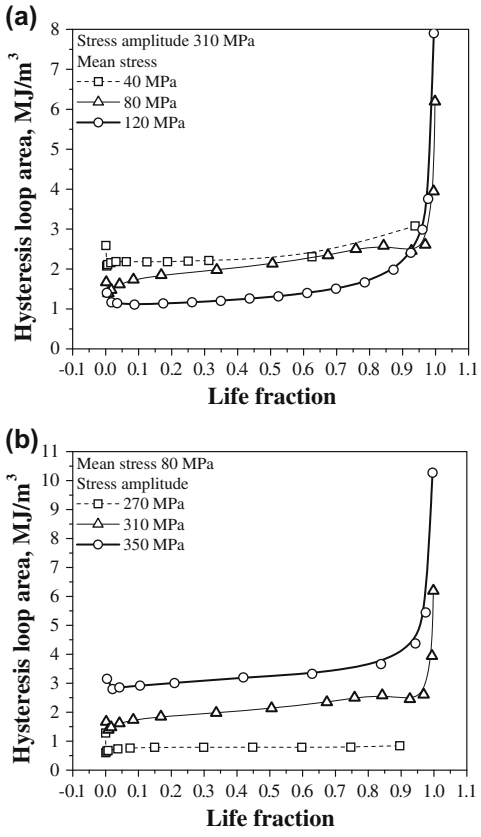

Fig. 10. Hysteresis loop area vs. life fraction: (a) at constant stress amplitude of 310 MPa and mean stress of 40, 80, and 120 MPa and (b) at constant mean stress of 80 MPa and stress amplitude of 270, 310, and 350 MPa.

During the time of investigating the cyclic response of materials, the effect of mean stress should be considered. The experiments are generally conducted in two different controlling modes: strain-controlled cycling with constant mean strain and stress controlled cycling with constant mean stress. If the material response is entirely elastic (high cycle fatigue), the above mentioned two types of tests are equivalent, and both can be used to study the effect of mean stress on the fatigue life of materials. On the other hand, if cyclic response of the material is elastic–plastic in nature, the above mentioned tests may produced different results. For strain cycling with mean strain, results relaxation of mean stress in the early stage of fatigue life will occur. Therefore the fatigue life is not appreciably affected by the introduction of a mean strain as compared with the symmetric strain cycling test [40,41]. Whereas, stress controlled cycling with mean stress causes accumulation of permanent strain (ratcheting strain) which impose an additional damage, resulting shorter in fatigue life [11,12,30,39]. So, ratcheting effects should be taken into account during prediction of fatigue life in case of asymmetric stress cycling.

During stress controlled fatigue, the accompanying variation in strain range with progression of cycles is due to the change in the hardening/softening response of the material. The evolving strain range is a function of the superimposed mean stress and can vary significantly through a test. Strain-based fatigue lifing approaches may not therefore be effectively employed for predicting stress controlled fatigue lives. Due to similar reasoning, energy based fatigue life prediction approaches are also not suitable. The inadequacy of strain based and energy based fatigue life prediction approaches are particularly apparent when the amount of plasticity is small and the hysteresis loop does not open up appreciably. It becomes imperative therefore to look towards stress-based approaches to

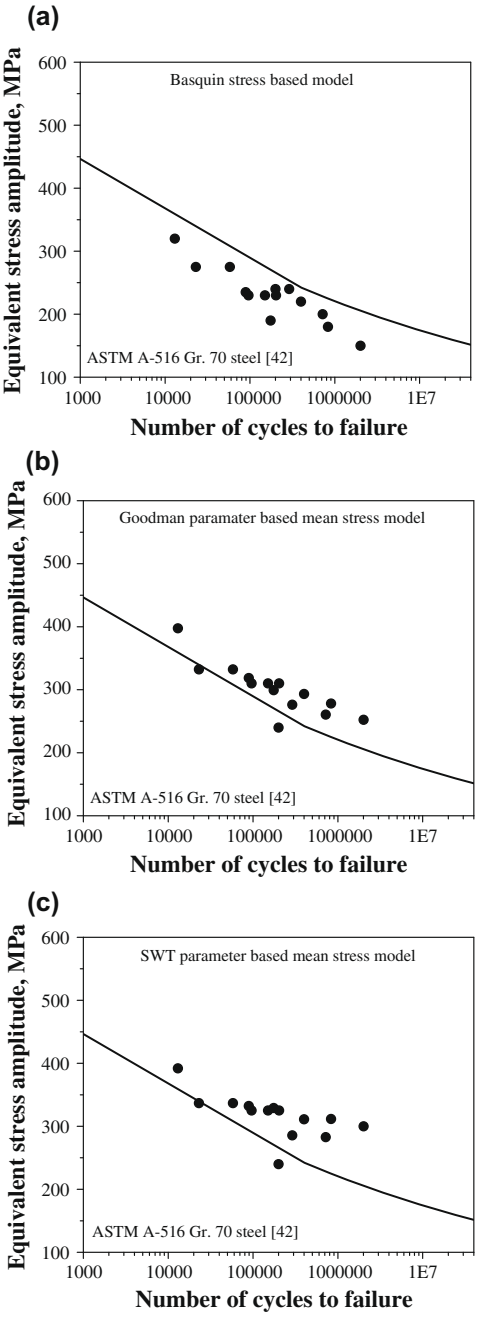

Fig. 11. Fatigue life prediction for different stress-based fatigue lifing equation with the fatigue data of ASTM A-516 Gr. 70 steel [42] by: (a) Basquin fatigue lifing equation, (b) Goodman parameter based fatigue lifing equation, and (c) Smith–Watson–Topper (SWT) parameter based fatigue lifing equation.

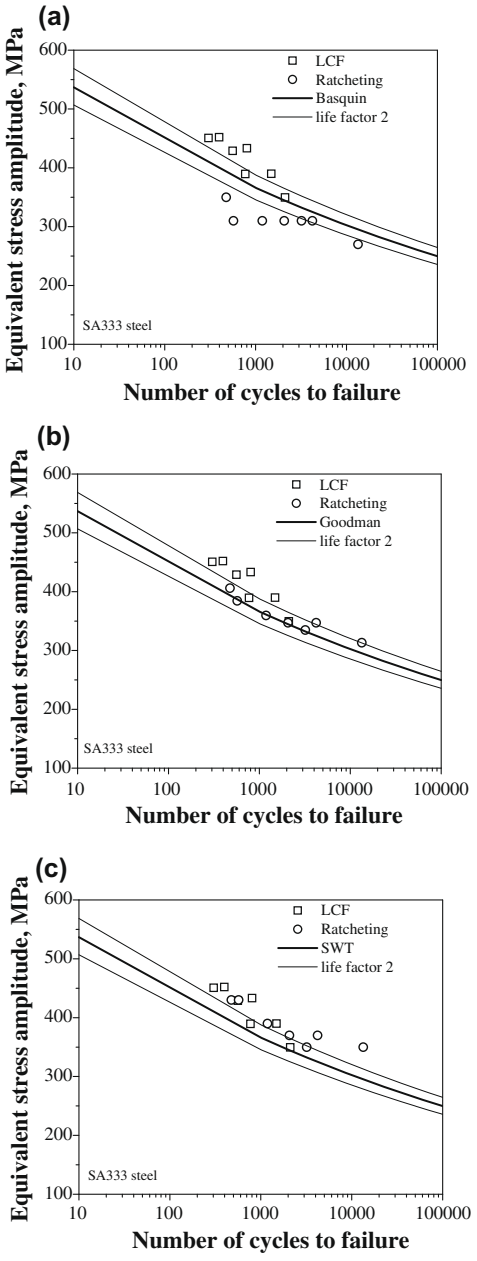

Fig. 12. Fatigue life prediction in SA333 steel for different stress-based fatigue lifing equation by: (a) Basquin fatigue lifing equation, (b) Goodman parameter based fatigue lifing equation, and (c) Smith–Watson–Topper (SWT) parameter based fatigue lifing equation.

model and predict fatigue lives under ratcheting conditions particularly, but extendable to all modes of fatigue cycling.

Under high cycle fatigue conditions, i.e. essentially for elastic stress controlled loading, the Basquin relation [8] is popular for modeling fatigue life. It is a power law relation given by

$$\sigma_a = \sigma'_f (N_f)^b \tag{4}$$

where σ_a, σ'_f and N_f are the stress amplitude, fatigue strength coefficient, and number of cycles to failure respectively. The exponent b has been related to the cyclic strain hardening exponent n' through

$$b = \frac{-n'}{1+5n'} \tag{5}$$

The Basquin relation was developed for fully reversed uniaxial stress cycling. In order to incorporate the effect of mean stress, a number of approaches are available, popular amongst which are the Goodman equation [9], modified Goodman equation [7], and Smith–Watson–Topper (SWT) parameter based equation [10]. All of these approaches attempt to formulates on equivalent stress amplitude σ_a^{eq} that can be substituted for σ_a in the Basquin relationship given in Eq. (4).

Some of the alternative formulations of σ_a^{eq} are:

Goodman equation:

$$\sigma_a^{eq} = \sigma_a \left(1 + \frac{\sigma_m}{\sigma_u}\right) = \sigma'_f (N_f)^b \tag{6}$$

Table 4
Material constants for proposed mean stress-based fatigue lifing equation.

Material	Reference	K (MPa)	n
SA333 C–Mn steel	Generated by us	756.2	−0.0969
Carbon Steel-45	Xianjie Yang [43]	934	−0.104
Copper alloy Elbrodur-NIB	Lim et al. [11]	1284	−0.117
ASTM A-516 Gr. 70 steel	Xia et al. [42]	1216	−0.114

Smith–Watson–Topper (SWT) parameter based equation:

$$\sigma_a^{eq} = \sqrt{\sigma_{\max}\sigma_a} = \sigma_a\sqrt{1+\frac{\sigma_m}{\sigma_a}} = \sigma_f'(N_f)^b \tag{7}$$

where σ_m, σ_u, and $\sigma_{\max}$ are the mean stress, ultimate tensile stress and maximum tensile stress of a particular cycle respectively. It may be noted that the equivalent stress amplitude σ_a^{eq} calculated as per any of the above methods is related to the fatigue life N_f through Eq. (4) with the constants σ_f' and b defined as per the Basquin relation.

In order to assess the efficiency of prevalent elastic stress-based approaches to model cyclic plastic fatigue life, a comparative study was carried out using the fatigue data of Xia et al. [42] for ASTM A-516 Gr. 70 steel. For this steel σ_f' was calculated as 903.3 MPa and b as −0.102. Fig 11a–c have shown the fatigue life plot for Basquin, Goodman, and Smith–Watson–Topper (SWT) lifing equations. None of these lifing equations are able to predict fatigue life satisfactorily for ASTM A-516 Gr. 70 steel. Of course, Basquin relation was formulated for fully reverse elastic cycling (HCF) only, so with onset of plasticity it does not work well. Similarly, Goodman equation which was also formulated for elastic stress cycling in presence of mean stress, does not predict fatigue life well in the presence of plasticity. One of the primary reasons for inability to predict fatigue life in the plastic domain by Goodman and SWT equations are, the use of same power law coefficient (σ_f') and exponent (n') which were introduced for HCF life prediction. So, this power law coefficient and exponent should be re-adjusted for the fatigue life prediction in plastic domain.

Equivalent stress amplitude in SWT equation is a function of σ_m to σ_a ratio. So, equivalent stress amplitude is dependent on σ_m/σ_a, not on the individual values of σ_m and σ_a, and as a result, low values of σ_m and σ_a and high values of σ_m and σ_a provide same responses which are not true. The SWT equation failed to predict ratcheting life especially at the high value of σ_m and low value of σ_a which is shown in Fig. 11c. Equivalent stress amplitude in Goodman equation is a function of σ_m to σ_u ratio. This Goodman lifing equation shows very low response at the condition of high stress amplitude and low mean stress, but it shows better result than SWT mean stress-based fatigue lifing equation which is shown in Fig. 11b. Similarly for SA333 steel, Fig 12a–c have shown the fatigue life plots for Basquin, Goodman and Smith–Watson–Topper (SWT) lifing equations respectively. For SA333 steel, power law coefficient (σ_f') and exponent (b) are 650 MPa and −0.08307. So above said figures clearly demand the re-tuning of power law coefficient and exponent in the fatigue lifing equation to predict fatigue life in the presence of cyclic plasticity.

To improve the response of mean stress (σ_m) on fatigue life prediction, equivalent stress amplitude, used in Goodman equation can be modified as:

$$\sigma_a^{eq} = \sigma_a\left(1+\frac{\sigma_m}{\sigma_{fl}}\right) \tag{8}$$

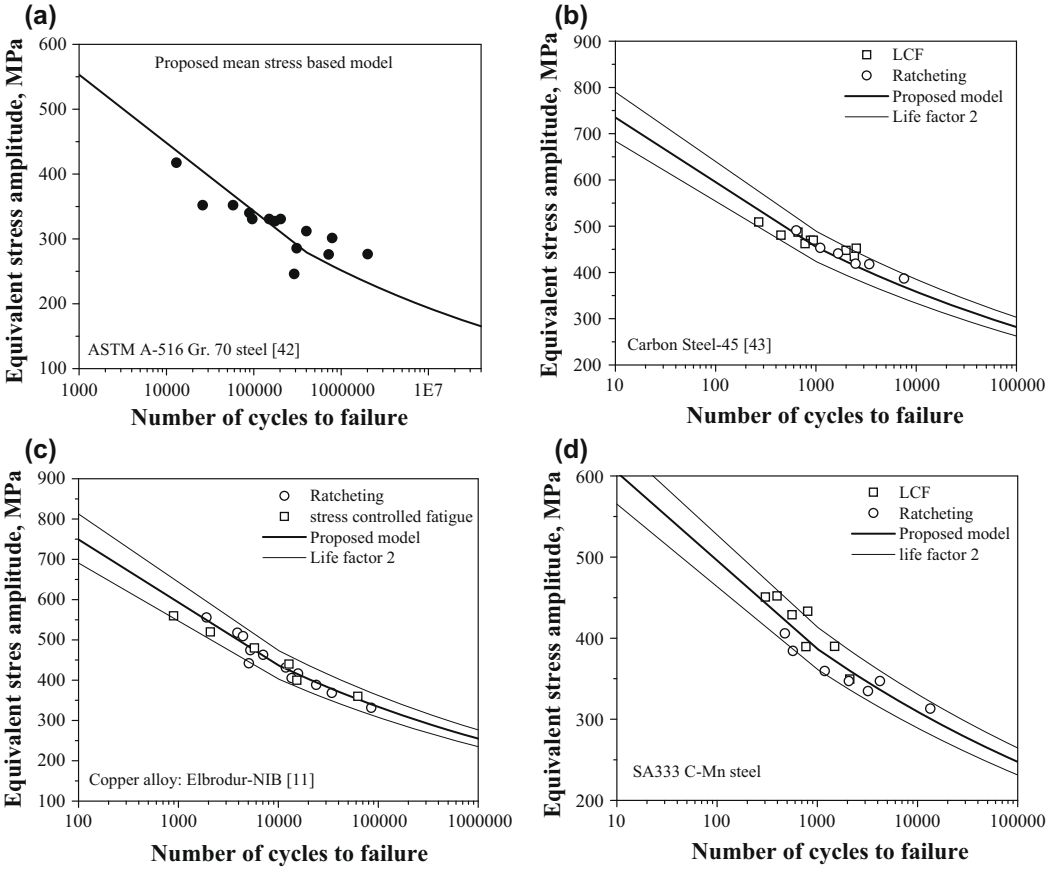

Fig. 13. Ratcheting and LCF life prediction by proposed mean stress-based fatigue lifing equation for the materials of: (a) ASTM A-516 Gr. 70 steel [42], (b) Carbon Steel-45 [43], (c) copper alloy: Elbrodur-NIB [11], and (d) SA333 C–Mn steel.

where σ_{fl} is the average flow stress which can be expressed as:

$$\sigma_{fl} = \frac{\sigma_y + \sigma_u}{2} \tag{9}$$

where σ_y is the yield stress.

Above discussion stipulates that power law coefficient (σ_f') and exponent (b), used in stress-based fatigue lifing equation (Eqs. (4), (6), and (7)), that was proposed to use in elastic stress cycling, are not valid with onset of plasticity. So, by redefining the power law coefficient (K) and exponent (n), fatigue lifing equation can be expressed as:

$$\sigma_a^{eq} = \sigma_a\left(1 + \frac{2\sigma_m}{\sigma_y + \sigma_u}\right) = K(N_f)^n \tag{10}$$

where K and n are the material constants. Essentially, K is true fracture stress (σ_f) and n is fatigue strength exponent (b) for Basquin, Goodman and SWT fatigue lifing equations. In the proposed fatigue lifing equation, material constants K and n can be determined from simple empirical equations: Eqs. (11) and (12). The Eqs. (11) and (12) are fully empirical and derived from solely experimental fatigue life data, fitting for different materials.

$$K = 17.5\sigma_y n' \tag{11}$$

$$n = \frac{1}{105}K^{0.35} \tag{12}$$

where n' is the cyclic strain hardening exponent. The proposed mean stress-based fatigue lifing equation is validated by four different materials. The values of material constants K and n are given in Table 4 for different materials. Fatigue life prediction by the proposed mean stress-based fatigue lifing equation are shown in Fig. 13a–d for the material of ASTM A-516 Gr. 70 steel [42], Carbon Steel-45 [43], copper alloy: Elbrodur-NIB [11] and SA333 C–Mn steel respectively. So it can be concluded from the above discussions after validating with four different metals that proposed mean stress-based fatigue lifing equation has the capability to predict ratcheting and LCF life in the range of 10^2–10^5 reasonably well.

4. Conclusions

From the above mentioned ratcheting and LCF study on SA333 steel, the following conclusions can be drawn:

(a) This material shows cyclic hardening throughout its LCF life.
(b) Ratcheting strain accumulation can be divided into three regions: primary, secondary, and tertiary.
(c) In engineering stress controlled ratcheting tests, specimens are failed by necking due to huge cross sectional area reduction.
(d) Ratcheting strain rate increases with increase in mean stress or stress amplitude.
(e) It is found in ratcheting tests that the plastic strain amplitude and hysteresis loop area decrease in the presence of mean stress.
(f) Proposed fatigue lifing equation predicts the ratcheting and LCF life in the range of 10^2–10^5 cycles well.

Acknowledgements

Our sincere thanks to Council of Scientific and Industrial Research (CSIR), New Delhi, India for awarding the Senior Research Fellowship to Mr. Surajit Kumar Paul and financially supporting him in the pursuance of his research study. The authors wish to thank The Director, National Metallurgical Laboratory, Jamshedpur, India for providing all the necessary facilities in carrying out this study.

References

[1] C. Gaudin, X. Feaugas, Acta Mater. 52 (2004) 3097.
[2] H.J. Roven, E. Nes, Acta Metall. Mater. 39 (1991) 1719.
[3] M. Petrenec, J. Polák, K. Obrtlík, J. Man, Acta Mater. 54 (2006) 3429.
[4] C. Sommer, H. Mughrabi, D. Lochner, Acta Mater. 46 (1998) 1537.
[5] H. Mughrabi, Acta Metall. 31 (1983) 1367.
[6] S. Bari, T. Hassan, Int. J. Plast. 16 (2000) 381.
[7] J.D. Morrow, ASTM STP 378, 1965, pp. 45–87.
[8] O.H. Basquin, Proc. ASTM 10, 1910, pp. 625–30.
[9] J. Goodman, Mechanics Applied to Engineering, Longmans Green, London, 1899.
[10] K.N. Smith, P. Watson, T.H. Topper, J. Mater. JMLSA 5 (1970) 767.
[11] C.B. Lim, K.S. Kim, J.B. Seong, Int. J. Fatigue 31 (2009) 501.
[12] S. Kwofie, Int. J. Fatigue 23 (2001) 829.
[13] M.S. Rahman, T. Hassan, E. Corona, Int. J. Plast. 24 (2008) 1756.
[14] T. Hassan, Y. Zhu, V.C. Matzen, Int. J. Pres. Ves. Pip. 75 (1998) 643.
[15] P. Carter, Int. J. Pres. Ves. Pip. 82 (2005) 27.
[16] T. Hassan, S. Kyriakides, Int. J. Plast. 10 (1994) 149.
[17] G. Li, M.N. Berton, Int. J. Pres. Ves. Pip. 54 (1993) 363.
[18] K. Thomas, Nucl. Eng. Des. 116 (1989) 199.
[19] Y. Jiang, H. Sehitoglu, Int. J. Plast. 10 (1994) 579.
[20] A. Mateo, L. Llanes, L. Iturgoyen, M. Anglada, Acta Mater. 44 (1996) 1143.
[21] X.L. Song, G.X. Yang, S.L. Zhou, H. Fan, S.S. Yang, J.W. Zhu, Y.N. Liu, Mater. Sci. Eng. A 483 (2008) 211.
[22] F. Lorenzo, C. Laird, Acta Metall. 32 (1984) 681.
[23] M. Bayerlein, H.J. Christ, H. Mughrabi, Mater. Sci. Eng. A 114 (1989) L11.
[24] S. Ganesh Sundara Raman, K.A. Padmanabhan, Int. J. Fatigue 17 (1995) 271.
[25] T.S. Srivatsan, S. Anand, J.D. Troxell, Int. J. Fatigue 15 (1993) 355.
[26] M. Botshekan, S. Degallaix, Y. Desplanques, J. Polak, Fatigue Fract. Eng. Mater. Struct. 21 (1998) 651.
[27] B. Wilshire, H. Burt, Int. J. Pres. Ves. Pip. 85 (2008) 47.
[28] H.X. Shang, H.J. Ding, Eng. Fract. Mech. 54 (1996) 1.
[29] Y. Jiang, J. Zhang, Int. J. Plast. 24 (2008) 1481.
[30] S.J. Park, K.S. Kim, H.S. Kim, Fatigue Fract. Eng. Mater. Struct. 30 (2007) 1076.
[31] S. Floreen, H.W. Hayden, Scripta Metall. 4 (1970) 87.
[32] K.S. Han, H. Margolin, Mater. Sci. Eng. A 112 (1989) 133.
[33] H.J. Christ, C.K. Wamukwamba, H. Mughrabi, in: X.R. Wu, Z.G. Wang (Eds.), Fatigue 99, Higher Education Press, Beijing, 1999, p. 2165.
[34] V. Kliman, M. Bily, Mater. Sci. Eng. 44 (1980) 73.
[35] H. Mughrabi, H.J. Christ, ISIJ Int. 37 (1997) 1154.
[36] A.P.L. Turner, T.J. Martin, Metall. Trans. A 11 (1980) 475.
[37] R. Eckert, C. Laird, J. Bassani, Mater. Sci. Eng. 91 (1987) 81.
[38] P. Lukas, L. Kunz, Int. J. Fatigue 11 (1989) 55.
[39] C. Holste, W. Kleinert, R. Gurth, K. Mecke, Mater. Sci. Eng. A 187 (1994) 113.
[40] F. Ellyin, ASME J. Eng. Mater. Technol. 107 (1985) 119.
[41] S.K. Koh, R. Stephens, Fatigue Fract. Eng. Mater. Struct. 14 (1991) 413.
[42] Z. Xia, D. Kujawski, F. Ellyin, Int. J. Fatigue 18 (1996) 335.
[43] X. Yang, Int. J. Fatigue 27 (2005) 1124.